The Effect of Water Filling Level in a Live-Bait Tank on the Stability of a 20 GT Pole and Line Fishing Vessel

Ummi H. Kalsum
Department of Naval Architecture, Hasanuddin University, Makassar, Indonesia
ummiikals@gmail.com

Daeng Paroka
Department of Ocean Engineering, Hasanuddin University, Makassar, Indonesia
dparoka@eng.unhas.ac.id (corresponding author)

Andi Nadia Himaya
Department of Naval Architecture, Hasanuddin University, Makassar, Indonesia
andinhimaya@gmail.com

Budimawan
Department of Marine Science, Hasanuddin University, Makassar, Indonesia
budimawan@unhas.ac.id

Fuad Mahfud Assidiq
Department of Ocean Engineering, Hasanuddin University, Makassar, Indonesia
assidiqfm@unhas.ac.id

Sabaruddin Rahman
Department of Ocean Engineering, Hasanuddin University, Makassar, Indonesia
sabaruddin-r@eng.unhas.ac.id

Andi Haris Muhammad
Department of Marine Engineering, Hasanuddin University, Makassar, Indonesia
andi_haris@ft.unhas.ac.id

Ahmad Fitriadhy
Program of Naval Architecture, Faculty of Ocean Engineering and Technology, Universiti Malaysia Terengganu, Mengabang Telipot, Kuala Nerus, Terengganu, Malaysia
naoe.afit@gmail.com

Alamsyah
Department of Naval Architecture, Kalimantan Institute of Technology, Balikpapan, Indonesia
alamsyah@lecturer.itk.ac.id

St. Aisjah Farhum
Department of Marine Science, Hasanuddin University, Makassar, Indonesia
aisjahfarhum@unhas.ac.id

Muammar Kadafi
Department of Ocean Engineering, Hasanuddin University, Makassar, Indonesia
kadafim22@student.unhas.ac.id

Siska
Department of Ocean Engineering, Hasanuddin University, Makassar, Indonesia
siskas22d@student.unhas.ac.id

Received: 8 December 2025 | Revised: 12 January 2026 and 28 January 2026 | Accepted: 29 January 2026

 DOI: https://doi.org/10.48084/etasr.16811

ABSTRACT

The stability of pole-and-line fishing vessels equipped with a live-bait tank is heavily influenced by the free surface effect caused by the water load. The sloshing motion of the load inside the tanks can increase the dynamic pressure on the tank walls and generate heeling moments (M_h) that may reduce the vessel's stability. This study aims to analyze the effects of water filling level (H) variation, roll excitation frequency, and roll angle (θ) on the distribution of hydrostatic and dynamic pressures, and their implications for vessel stability. Numerical simulations were conducted using Computational Fluid Dynamics (CFD) in the Ansys Fluent with the Volume of Fluid (VOF) method in a hull-shaped tank under transient conditions. A dynamic mesh was applied to track the fluid-free surface, and a pressure-based solver employing the k-ω Shear Stress Transport (SST) turbulence model was used and verified through a grid-independence test. The simulations were performed for H between 10% and 90% of the tank height, roll excitation frequencies between 0.5 and 2.5 rad/s, and θ between 5 ° and 20 °. The results showed that the highest dynamic pressure values were recorded near the free surface under all filling conditions. Roll frequency and θ significantly affected the pressure when the H in the tank was approximately 50% of the tank height. At an H of 90%, the pressure on the tank walls did not show any significant variation. Compared to the low filling condition (10%), the average sloshing pressure increased by more than one order of magnitude as H approached 70% of the tank height. The M_h induced by water pressure on the tank walls increased with higher H and with the ratio of free surface height to width. The representative sloshing-induced M_h increased by approximately 85% at a 90% filling level compared to the 10% filling condition. The lowest gradient of M_h increase occurred at water levels between 50% and 70%, corresponding to a free-surface height-to-width ratio of 0.21–0.27. The influence of resonant frequency on the disturbing arm (GZ_h) was more pronounced when the H was below 50% of the tank height than at higher H. The maximum GZ_h of 0.013 m occurred at an H of 90%, with a roll frequency of 2.5 rad/s and a θ of 20 ° corresponding to the reduction of righting arm (GZ_r) of 1.82% of the original. These results indicated that the vessel maintained sufficient stability to counteract the M_h generated by the water motion within the live-bait tank.

Keywords-vessel stability; sloshing; heeling moment; free-surface effect; filling level; CFD

I. INTRODUCTION

Tuna is a globally distributed fishery commodity with significant commercial and economic value [1, 2]. The total annual tuna production using pole-and-line fishing gear averaged over 360 tons during the 2011–2013 period [3]. This production is expected to continue to increase in the future. The pole-and-line technique utilizes live-bait to catch fish such as tuna. Pole-and-line fishing vessels are equipped with live-bait tanks to maintain the bait's viability throughout the fishing operation. According to [4], the survival of live bait for a certain period depends on several factors, including stocking density, water quality, circulation, and illumination. The live-bait tank is installed within the ship's hull and filled with seawater to a specific volume to ensure continuous water circulation. During operation, the filling level of the live bait tank should be reduced to maintain the vessel draught due to additional weight induced by the fish catch. Partially filled live-bait tanks affect the operational performance of the vessel, particularly its stability [5]. The free surface of the tank contributes to a reduction in Metacentric Height (GM) due to an increase in the height of the center of gravity. The wider the free surface, the greater the reduction in GM [6]. Conversely, for the same free surface width, a larger tank volume results in a smaller GM correction due to the free surface effect. Small to medium-sized pole-and-line fishing vessels with cross-sectional shapes approaching an extreme V-form are more susceptible to the free surface effect. This is attributed to the lower tank volume compared to vessels with rectangular cross-sections, while maintaining the free surface width.

During operation, the water inside the live-bait tank moves in response to the ship's motion. This water movement creates dynamic pressure on the tank walls, generating a M_h that can affect the vessel's stability [7]. The magnitude of this M_h depends on the water velocity upon impact with the wall, the cross-sectional area of the tank wall, and its distance from the ship's center of gravity. When the phase of the water motion inside the tank coincides with the phase of the vessel's rolling motion, the resulting heel angle can increase. In some cases, sloshing may generate additional damping moments that reduce roll amplitude, as observed in CFD simulations for an ONR Tumblehome hull with a partially filled tank under regular head

waves [8]. The dynamic effects of water motion inside a tank depend strongly on the ship's operating environment such as wave conditions and encountered frequency. This is supported by experimental and numerical investigations of liquid tank sloshing under regular waves [9]. It was revealed that the most violent sloshing occurs at frequencies below the tank's natural frequency, highlighting the sensitivity of sloshing intensity to wave characteristics and tank hydrodynamics. In addition, tank geometry and filling level significantly influence the intensity of sloshing and the resulting dynamic pressure on the tank walls [8].

The vessel's θ and roll period highly affects the dynamic behavior of tank content, including the pressure acting on the tank walls. CFD simulations of parametric roll with more violent sloshing potentially led to higher pressure values [8]. Similarly, simulations using the MPS method for complex ship tanks indicate that roll amplitude and period control the magnitude of sloshing-induced forces on the tank [10]. A larger θ produces higher pressure on the tank walls, while an increase in the roll period also leads to higher pressure, though the effect is less significant than that of θ variation. Furthermore, sloshing in the tank affects the natural roll frequency of the vessel, which in turn alters the roll amplitude and rolling moment. Authors in [11] observed that sloshing alters the natural roll frequency of medium-sized liquid-carrying vessels, amplifying roll when wave frequency approaches resonance, especially at medium filling levels (0–0.8). Authors in [12], using SPH simulations for the S175 containership and membrane LNG carriers, also confirmed a similar phenomenon. Specifically, when the wave frequency approaches the natural frequency of the tank, resonance occurs, increasing dynamic pressure on the tank walls, θ, and roll period, with tank geometry and filling level being critical factors. Additionally, authors in [13] emphasized that for large LNG carriers, sloshing affects roll damping, roll amplitude, and tank pressure, with the effect being highly sensitive to wave heading and filling level.

The water level inside the live-bait tank of a pole-and-line fishing vessel can vary during fishing operations and is dependent on bait density and loading conditions. Small to medium-sized vessels are subject to more significant performance variations due to sloshing effects than larger ships. Research on the hydrodynamic behavior of the live-bait tank's water, particularly in relation to vessel stability, remains limited. Authors in [14] investigated the use of floating baffles to mitigate the sloshing effect inside the tank of traditional Indonesian fishing vessels. This finding suggested that sloshing significantly influences the rolling motion of small fishing vessels.

To enhance the operational performance of pole-and-line fishing vessels, understanding the effect of sloshing on their stability is essential. By analyzing this phenomenon, the tank configuration can be optimized according to the characteristics of the operating environment and minimize excessive sloshing effects. The outcomes of this study can contribute to the design of live-bait tanks for pole-and-line vessels that can simultaneously function as anti-roll tanks, thereby improving stability performance while maintaining the requirements and criteria for bait survival.

II. METHODOLOGY

A. *Fishing Vessel Data*

The data utilized in this study consist of the offset of hull form of the ship to develop the bait tank model, the dimension of the bait tank, the vertical center of gravity corresponds to the rotation axis for the tank simulation, and the GZ_r for the stability margin evaluation means. The main dimensions of the vessel and the live-bait tank are presented in Table I.

TABLE I. DIMENSIONS OF THE FISHING VESSEL AND LIVE-BAIT TANK

Parameter	Abbreviation	Value (m)
Length overall	LOA	22.8
Length between perpendiculars	LBP	18.99
Breadth	B	4.8
Height	H_s	1.6
Draft	T	1.12
Vertical center of gravity	VCG	1.12
Length of life bait tank	L	4.6
Wide of live-bait tank	b	4.6
Height of live-bait tank	h	1.6

The vessel described in Table I is chosen as a sample ship due to its similarity to most of the pole-and-line fishing vessels operating in Indonesia. The hull form of the vessel, as well as the shape and position of the tank are illustrated in Figure 1.

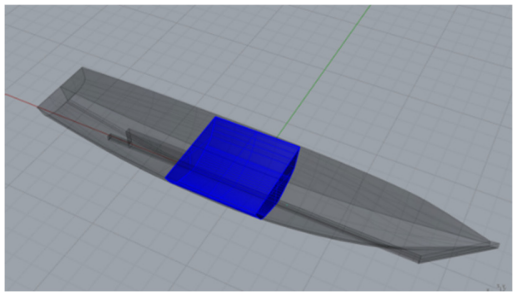

Fig. 1. Model of the vessel including hull form, tank shape, and position.

The GZ_r curve of the vessel without the effect of tank-induced load is depicted in Figure 2.

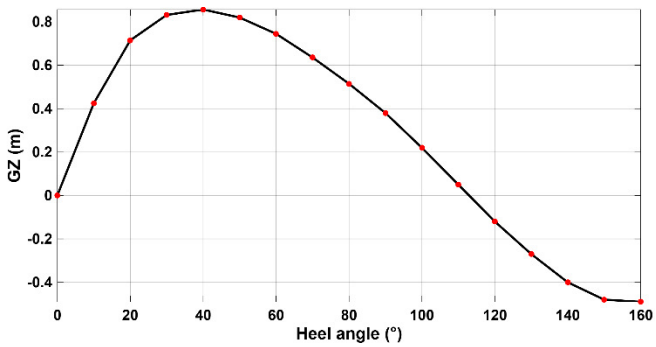

Fig. 2. GZ_r curve of the vessel.

The geometry of the life bait tank follows the hull form with the same height as the vessel's and is in the longitudinal position of 8.45 m up to 13.05 m from the stern end. Those data were obtained by direct field measurement in a wooden boat shipyard in Indonesia and have been used in previous research including the GZ_r curve of the ship [15], as presented in Figure 2.

B. Simulation Variations

Simulations were performed to investigate the effects of tank geometry and filling level on sloshing loads. The simulations utilized several water levels inside the tank (10%, 30%, 50%, 70%, and 90% of the tank height) following previous studies conducted on different ships, including the 17,500 LTDW tanker [16] and a general-purpose tanker [17]. These variations not only affect tank filling but also alter the width of the free water surface, since the tank is not rectangular.

The influence of ship motion characteristics on the sloshing phenomenon when the vessel experiences roll motion with frequencies lower or higher than the roll natural frequency of the ship was studied. These frequencies include values of 0.5 rad/s, 1.0 rad/s, 1.519 rad/s, 2.0 rad/s, and 2.5 rad/s. The rolling angles are assumed to be 5 °, 10 °, 15 °, and 20 °. For higher θ, the vessels cannot safely operate. The sloshing simulation is performed for the live-bait tank without considering the coupling effect between ship motion and sloshing response. Therefore, the effect of external forces such as waves of the ship motion is not considered.

C. Mathematical Model

The water dynamics inside the live-bait tank were analyzed by CFD using Ansys Fluent, governed by the conservation of mass and momentum through the Navier–Stokes equations, following the formulation presented in [18]. These equations describe the variations in mass flow and the forces acting on the fluid because of interactions among momentum, pressure, and viscous stresses.

1) Continuity Equation

$$\frac{\partial \rho}{\partial t} + \nabla \cdot (\rho \vec{v}) = 0 \quad (1)$$

where ρ is the density of the fluid inside the live-bait tank and $\vec{v}$ is the fluid velocity vector.

2) Momentum Equation (Transient Navier–Stokes)

$$\frac{\partial}{\partial t}(\rho \vec{v}) + \nabla \cdot (\rho \vec{v}\vec{v}) = -\nabla p + \nabla \cdot [\mu(\nabla \vec{v} + \nabla \vec{v}^T)] + \rho \vec{g} + \vec{F} \quad (2)$$

where p denotes pressure, μ is the dynamic viscosity, $\vec{g}$ is the gravitational acceleration, and $\vec{F}$ represents external body forces acting on the fluid. The operator ∇ denotes the gradient operator, representing the spatial derivative used to describe variations in a physical quantity, such as velocity or pressure, within the fluid flow field.

In this study, the external force $\vec{F}$ was not directly applied, as the fluid motion was entirely driven by the tank wall movement. The latter was assigned a moving boundary condition corresponding to the vessel's roll motion. At the tank wall surface, a Dirichlet (no-slip) boundary condition was applied, assuming that the fluid velocity was zero relative to the wall.

3) Turbulence Model k-ω SST

The sloshing phenomenon within the live-bait tank involves complex interactions between the free surface motion, sharp velocity gradients, and wall–fluid interactions. To accurately capture these effects, the $k-\omega$ SST turbulence model developed in [18], was deployed. This model combines the advantages of the $k-\omega$ formulation in predicting near-wall boundary layers with those of the k-ϵ model in the free-stream region away from the wall. Mathematically, the transport equation for the turbulence kinetic energy (k) in the $k-\omega$ SST model is modified as presented in (3), with the modification terms shown by (4) and (5):

$$\frac{\partial(\rho k)}{\partial t} + \frac{\partial(\rho k u_i)}{\partial x_i} = \frac{\partial}{\partial x_j}\left(\Gamma_k \frac{\partial k}{\partial x_j}\right) + G_k^* - Y_k^* + S_k \quad (3)$$

$$G_k^* = \gamma_{eff} \tilde{G}_k \quad (4)$$

$$Y_k^* = \min\left(\max\left(\gamma_{eff}, 0.1\right), 1.0\right) Y_k \quad (5)$$

where k is the turbulence kinetic energy, u_i is the velocity component in the i-direction, and Γ_k is the effective diffusivity of k. S_k is the source term, G_k^* is the corrected turbulence production term, and Y_k^* is the corrected turbulence dissipation rate.

The correction terms for G_k and Y_k are governed by the blending function (γ_{eff}), allowing the model to adaptively combine the characteristics of $k-\omega$ near the wall and $k-\epsilon$ in the free-stream region. This hybrid formulation makes the $k-\omega$ SST model numerically stable and more accurate for free-surface flows with moving boundaries, such as the sloshing motion within the live-bait tank of fishing vessels.

4) Boundary Conditions

All tank walls were modeled as rigid bodies moving relative to an inertial reference frame using a dynamic mesh approach. The roll motion was applied employing User-Defined Function (UDF), causing all tank walls to oscillate according to the specified function. This function provides an angular velocity $\dot{\theta}(t) = a_1 \omega \cos(\omega t)$, corresponding to the $\theta(t) = a_1 \sin(\omega t)$ with the axis of rotation located at the vessel's center of gravity, 0.7 of the ship height measured from the baseline. This center of rotation is applied for all simulation scenarios. The wall friction boundary was set as a no-slip wall, ensuring that the fluid velocity at the wall matches the moving wall velocity. The top surface of the tank was defined as a free surface, and there were no inlets or outlets, as the tank is considered closed.

5) Volume of Fluid

The VOF method is a numerical technique used to track the interface between fluids. Equations (6) and (7) express the conservation of the volume fraction of phase q (water or air). For the sloshing case without phase change, source terms and

interphase mass transfer are assumed to be zero, simplifying the VOF equations to the conservative advection form for α_q:

$$\frac{\partial \alpha_q}{\partial t} + \nabla.(\alpha_q u) = 0 \quad (6)$$

$$\sum_{q=1}^{n} \alpha_q = 1 \quad (7)$$

In the VOF method, the scalar function $F(x, y, z)$ identifies each cell as air ($F = 0$), water ($F = 1$), or a mixture at the free surface ($0 < F < 1$), ensuring that the total volume fraction remains conserved. The fluid properties in each control volume are determined based on the volume fraction of each phase, with the mixture density for a two-phase system calculated by:

$$\rho = \alpha_2 \rho_2 + (1 - \alpha_2)\rho_1 \quad (8)$$

In general, for n phases, properties such as density and viscosity are computed as a weighted average based on the volume fractions, as expressed in:

$$\rho = \sum \alpha_q \rho_q \quad (9)$$

In ANSYS Fluent, the VOF model solves a single momentum equation for the entire domain, with velocity u shared among phases according to (2).

6) Pressure

The pressure on the tank walls consists of hydrostatic pressure, which is a function of the water level in the tank and dynamic pressure. This is caused by the water motion and depends on the fluid velocity. The total pressure on the tank wall is expressed by:

$$P = \rho g h + \frac{1}{2}\rho v^2 \quad (10)$$

where P is the time-varying total sloshing pressure, and v is the fluid velocity resulting from the sloshing motion. Figure 3 presents the pressure measurement points along both directions of the vessel.

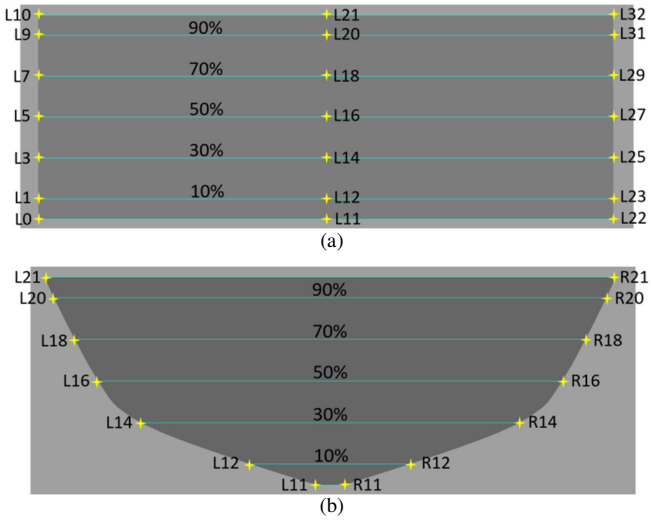

Fig. 3. Pressure measurement points: (a) along the longitudinal section of the tank, (b) along the transverse section of the tank.

Differences in water level result in variations in hydrostatic pressure and water motion velocity within the tank. Consequently, the dynamic pressure also varies with depth or distance from the free surface. Therefore, the water pressure on the tank walls was measured at multiple positions along the tank height and along the longitudinal direction of the tank, as shown in Figure 3(a) for the longitudinal section and Figure 3(b) for the transverse section. Pressure measurement points L0–L32 were located on the left side of the tank, while R0–R32 on the right side, as measured from the lowest position (tank bottom) to the highest position at the tank free surface.

D. Vessel Stability

A tank containing water affects the vessel's stability both statically and dynamically. Statically, the free surface of water inside the tank reduces the GM due to the inertia of the free surface. Dynamically, the water pressure on the tank walls generates moments that can reduce the vessel's righting moment. In [7], CFD simulations of tanks with varying dimensions highlight that the M_h generated by liquid sloshing depends on various parameters, including tank geometry, filling level, tank location within the hull, and the ship's rolling period. On the other hand, changing loading conditions, such as the gradual filling of tanks during operations, can generate excitation moments that increase the roll motion amplitude [19].

The sloshing force on tank walls is statically calculated following the approach proposed in [10], using:

$$F_i = \sum_{t=1}^{n} P_i(\Delta Z_i \,.\, W_i) \quad (11)$$

where n is the number of panels on the wall, P_i is the sloshing pressure on the i-th panel obtained by CFD simulation, ΔZ_i is the height of the i-th panel, and W_i is the length of the i-th panel.

This force then produces a M_h, which is the resultant of the transverse and vertical components of the forces from the pressure acting perpendicular to the tank wall panels, as expressed by:

$$M_h = M_x + M_y \quad (12)$$

$$M_x = \sum_{i=1}^{n} F_{xi} \cdot y_i \quad (13)$$

$$M_y = \sum_{i=1}^{n} F_{yi} \cdot x_i \quad (14)$$

where F_{xi} and F_{yi} are the transverse and vertical components of the sloshing-induced force on panel i, calculated using (15) and (16). Additionally, x_i is the transverse distance of the vertical force component from the vessel's center of gravity, and y_i is the vertical distance of the transverse force component from the center of gravity. If the transverse force component is above the center of gravity, y_i is positive; otherwise, it is negative.

$$F_{xi} = F_i \sin \varphi_i \quad (15)$$

$$F_{yi} = F_i \cos \varphi_i \quad (16)$$

where F_i is the force on each tank wall panel, obtained from (11), evaluated at the mid-panel, and φ_i is the inclination angle of the panel relative to the horizontal axis.

The M_h obtained from (12) must be smaller than the vessel's righting moment (M_r) to ensure that the ship is able to return to its upright position, as presented in Figure 2. Otherwise, anti-rolling equipment like an outrigger should be attached or the layout of ship equipment should be changed to preserve the ship's stability [20]. Authors in [21] studied Indonesian fishing vessels and revealed that the GZ_r is an indicator of stability and seakeeping of a ship. In this study, the dynamic M_h induced by live-bait tank sloshing is expressed as a disturbing arm, and can be determined using:

$$GZ_h = \frac{M_h}{\Delta} \quad (17)$$

E. Grid Independence

Prior to performing the main simulations, a grid independence test was conducted to ensure that the simulation results are not dependent on the number of mesh elements. The criterion for selecting the optimum mesh was when the changes in the average pressure on the tank walls become insignificant across different mesh levels. This test aims to determine a mesh size that provides stable computational results with an efficient computing time. The test was performed on several mesh sizes between 0.3 m and 0.03 m using the pressure on the tank walls as the reference parameter, as shown in Figure 4.

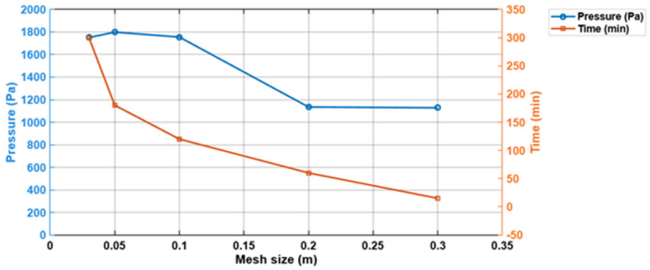

Fig. 4. Grid independence test curve.

The comparison results indicate that as the mesh size decreases, the calculated pressure approaches a converged value. The pressure obtained with a 0.1 m mesh (1755.0366 Pa) closely matched finer meshes, namely 0.05 m (1798.6623 Pa) and 0.03 m (1750.7485 Pa), with a relative difference of less than 3%. Based on considerations of accuracy and efficiency, a mesh size of 0.1 m was selected for the main simulations. This mesh size provides convergent results while keeping the total number of elements manageable (26,955 elements and 116,969 nodes) and the computation time relatively short (120 min).

The simulations were carried out over a 20-s transient period using ANSYS. The VOF method was employed to track the air–water interface and the dynamic mesh to capture the deformation of the free surface, as in previous 2D rectangular tank studies with varying geometries [16]. The boundary conditions included tank walls as no-slip walls and the fluid top surface as a free surface. The $k-\omega$ SST turbulence model was selected to accurately capture the turbulent eddies near sharp gradients and free surfaces, as demonstrated in high-fidelity flow simulations [22]. The PISO scheme was used to enhance pressure–velocity coupling and improve momentum conservation at each pressure-correction step, according to [23].

III. RESULTS AND DISCUSSION

A. Pressure on Tank Walls

The effect of filling level, roll motion frequency, and θ to the pressure on tank walls was investigated based on the fluid motion inside the tank, estimated by CFD simulation. In this study, the simulations were performed for the live-bait tank without dynamically coupled with the vessel motion induced by waves. The obtained pressures are used to statically calculte the induced M_h experience by the vessel.

1) Effect of Water Filling Level

Figure 5 visualizes the free surface dynamics and pressure distribution on the tank walls from the second to the twentieth s. The left panels illustrate the changes in the water surface shape (volume fraction). The right panels show the water pressure distribution. The red color pattern indicates high-pressure areas, and the blue pattern indicates low-pressure areas that appear when water waves impact the tank walls.

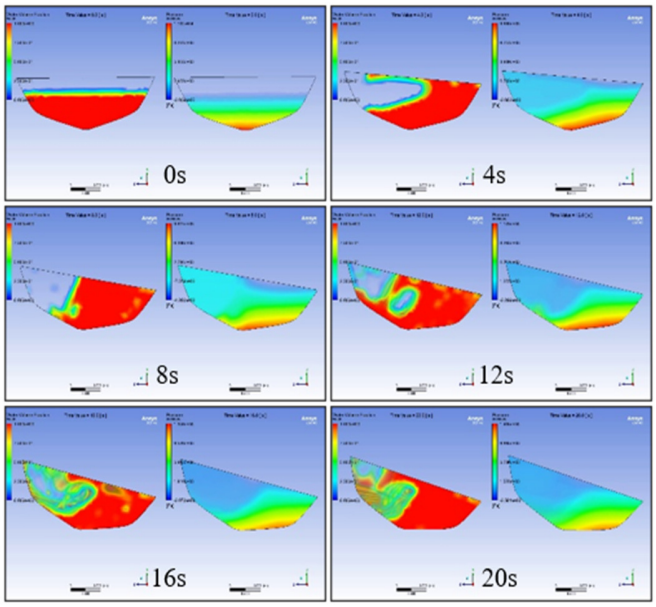

Fig. 5. Visual free surface and water pressure in the tank (H = 70%, roll frequency = 1.519 rad/s, and θ = 20 °).

Dynamic pressure peaks occur simultaneously with the water impact on the tank walls, which can be observed in Figure 5 and supported by the time series pressure results in Figure 6. At approximately 2.1 s, 6.2 s, 10.3 s, 14.5 s, and 18.6 s, water moves rapidly toward the left side of the tank, producing significant dynamic pressure spikes. Conversely, at approximately 1.1 s, 5.1 s, 9.3 s, 13.6 s, and 17.7 s, static pressure dominates due to low flow velocity, even though the water surface height is at its maximum.

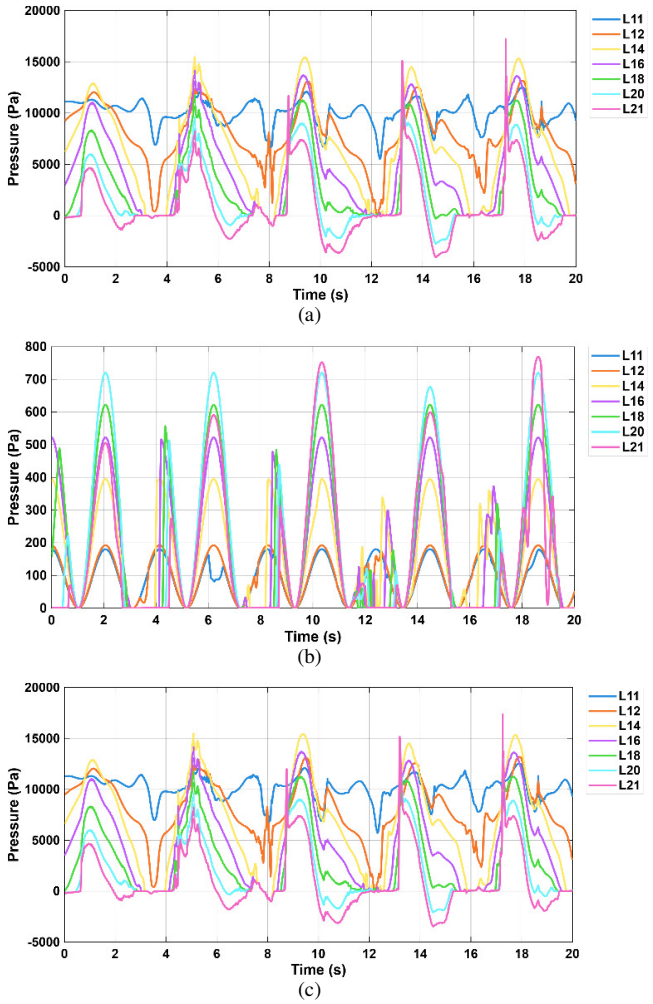

Fig. 6. Time-series of pressure: (a) static, (b) dynamic, and (c) total (H = 70%, roll frequency =1.519 rad/s, and θ = 20 °).

The phase shift between static and dynamic pressures is around 1 s, equivalent to 0.24 of the sloshing period (T ≈ 4.13 s), indicating a phase lag between the fluid's potential and kinetic energy. This condition suggests that the dynamic pressure peaks approximately a quarter of a period after the static pressure maximum, consistent with the 90 ° phase lag criterion in resonant sloshing phenomena. Experimental observations [24] in controlled sloshing tanks confirm the 90 ° phase lag predicted by theory, providing a reference for identifying response maxima and validating the dynamic pressure behavior in live-bait tanks. During resonance, the fluid motion always lags the excitation force by 90 °, regardless of the maximum energy conversion from potential to kinetic during one oscillation cycle. Therefore, the maximum total pressure during the water-impact phase was the main contributor to the lateral force on the tank walls. This force generates dynamic M_h that can potentially reduce the stability of the vessel, particularly when resonance occurs between the water motion and the vessel's rolling motion. Further discussion on the effect of this pressure on M_h and vessel stability is provided in the following section.

The simulation results illustrated in Figure 7 indicate that an increase in the H generally increases the total pressure on the tank walls. Under normal sloshing conditions, peak pressures typically occur at the lowest points of the tank walls, as observed in CFD simulations of LNG carrier tanks under roll excitation [25]. For instance, at measurement point L11, the total pressure increased from approximately 553 Pa (H = 10%) to 11,607 Pa (H = 90%). A similar pattern is observed at most measurement points, except at L12, where the pressure is smaller than at L14 for H of 10–50%. This phenomenon, at low filling levels, is attributed to the maximum pressure zone shifts upward toward the free surface due to the wave impact and the formation of up-rushing jets near the water surface [26].

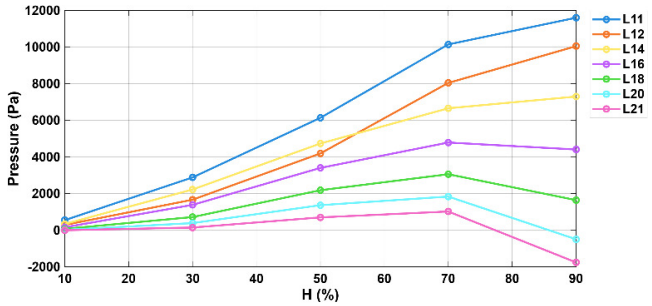

Fig. 7. H against total pressure (roll frequency = 1.519 rad/s and θ = 20 °).

Figure 8 displays the separation between the static and dynamic pressures on the tank walls for different H. Figure 8(a) shows the static pressure distribution, while Figure 8(b) portrays the dynamic pressure distribution. According to Figure 8(a), static pressure increases with rising water level according to $P_h = \rho g h$. This is attributed to the increased water column height, leading to greater weight on the tank, and therefore resulting in higher wall pressure. However, at measurement points near the free surface (L20 and L21) with 90% filling, the static pressure was recorded below zero. The effect of water level changes on static pressure at upper points was smaller than that at lower points (L11–L16).

Conversely, dynamic pressure, as presented in Figure 8(b), reveals a different pattern. At the tank bottom (L11–L12), variations in water filling have little effect on dynamic pressure due to the weak fluid motion in this region. However, near the free surface, dynamic pressure fluctuations increase as the oscillating water mass becomes larger and the flow velocity reaches its maximum, consistent with experimental observations of nonlinear sloshing behavior [27]. As the filling level approaches full capacity, the dynamic pressure begins to decrease because the free surface has limited space to oscillate, which reduces the sloshing amplitude and overall energy. This reduction of oscillation energy at higher filling levels is consistent with the structural-loading observations reported in [28]. A comparable depth-dependent weakening of sloshing response was also confirmed experimentally in [29]. Therefore, the dynamic pressure near the free surface reached a higher peak than that at the bottom, and subsequently decreased when the tank was almost full.

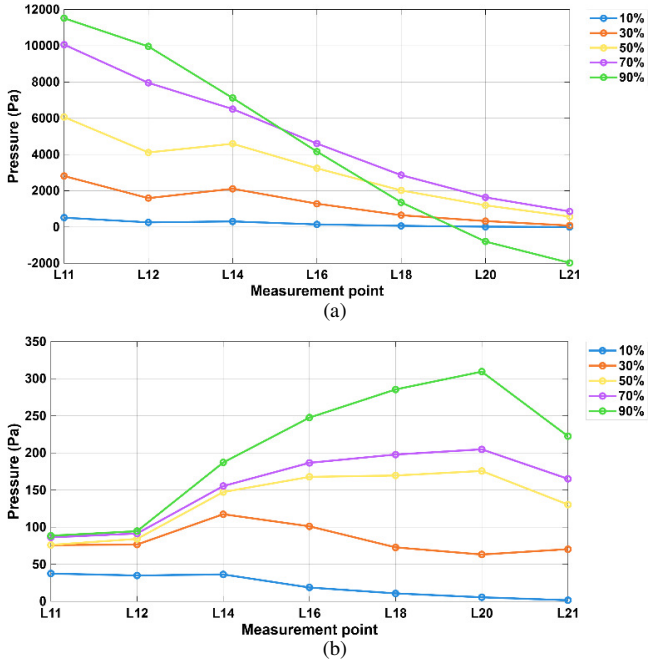

Fig. 8. H against pressure: (a) static and (b) dynamic (roll frequency = 1.519 rad/s and θ = 20 °).

The dynamic pressure serves as the basis for calculating the M_h, measured at L11–L21. The highest values of this pressure were observed at an H equal to 90%, due to the increasing oscillating water mass and the impact on the tank walls. At shallow water conditions (H between 10–30%), the low water volume limits the sloshing energy, whereas for $H \geq 50\%$, the amplitude and pressure distribution increase significantly, reaching a peak for an H between 70% and 90%. This finding aligns with [30], where it was reported that increasing the tank filling level significantly amplifies fluid hydrodynamic fluctuations and free surface displacement amplitude. Consequently, the mean total pressure becomes the maximum at medium water levels ($H \approx 70\%$), as the water mass is sufficiently high. Authors in [28, 29] observed that under very high filling conditions, the limited space for fluid motion accounts for the low total pressure on the tank walls at an H of 90% compared to moderate filling (H = 70%). Furthermore, authors in [11] emphasized that increasing the water height in the tank, lowers the vessel's natural roll frequency and increases the average dynamic loads, supporting the observation that H values between 70% and 90% represent the most significant condition for vessel structure and stability.

2) Effect of Roll Motion Frequency

The vessel's roll excitation frequency also affects the pressure distribution. In Figures 9(a) and 10, under half-filled conditions (H = 50%), the mean total pressure exhibits a non-monotonic peak as the roll frequency increases.

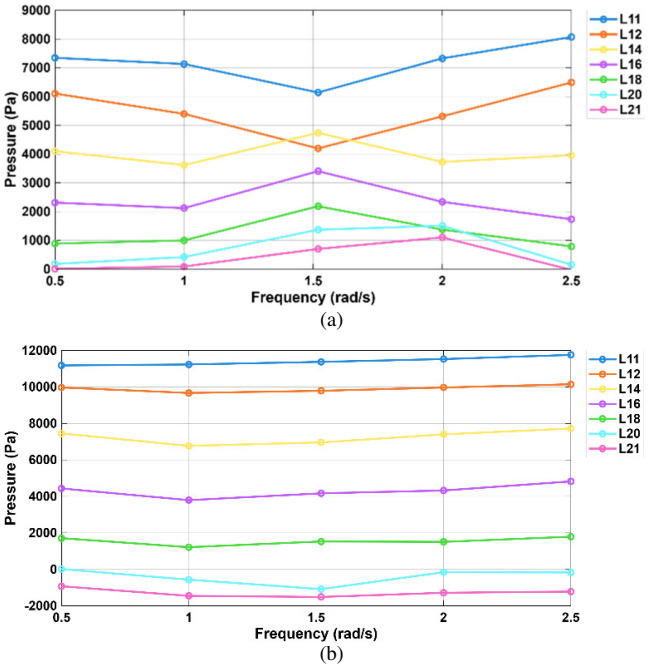

Fig. 9. Roll frequency against total pressure for: (a) $H$of 50% and (b) H of 90% (θ = 20 °).

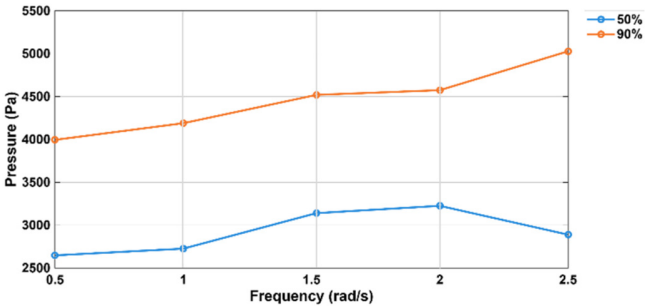

Fig. 10. Roll frequency and mean total pressure (θ = 20 °).

The highest pressure occurs at a frequency of 2 rad/s and then decreases at 2.5 rad/s due to the dominance of inertial effects. At low frequencies (0.5–2 rad/s), the water has sufficient time to follow the tank motion. The free surface oscillation amplitude can exhibit high values because the internal wave speed is relatively balanced with the vessel motion. Therefore, pressure increases with a frequency of up to nearly 2 rad/s (near-resonance phenomenon). Beyond the resonant condition (>2 rad/s), such as at 2.5 rad/s, the vessel motion becomes faster, and the water can no longer fully follow the movement due to its large mass (increased water inertia). As a result, the relative motion between the tank walls and the water mass decreases, reducing the sloshing amplitude. This behavior is consistent with [12], showing that when the excitation frequency approaches the natural frequency of water in the tank, the water motion amplitude and pressure increase. A similar tendency has been reported in previous numerical investigations of sloshing dynamics, where violent sloshing and intensified loads were observed near resonant excitation conditions [22]. The present results exhibit comparable

behavior, although differences in excitation modes and tank geometry lead to variations in the magnitude of the response. This indicates that internal wave modes can be preferentially excited at certain driving frequencies, producing distinct resonance patterns, consistent with the findings of [31], which demonstrated this behavior in a shallow-water rectangular tank.

In contrast, under near-full conditions (H = 90%), as shown in Figures 9(b) and 10, the total pressure increases monotonically with excitation frequency. This is attributed to the dominance of the large water mass and the limited free-surface movement. Consequently, the pressure response is primarily controlled by the water's inertial component ($P_d \propto v^2 \propto f^2$) rather than by sloshing motion. The free surface under high filling is relatively constrained, preventing the sloshing amplitude from developing significantly [28]. Since the inertial force is proportional to the square of the frequency ($F \sim \omega^2$), increasing the frequency results in higher average loads on the tank walls, even though sloshing amplitude is not dominant. The data show that the mean total pressure tends to increase monotonically with frequency.

Overall, the analysis results indicate that the excitation frequency directly affects vessel stability through variations in pressure caused by sloshing motion inside the tank. Maximum pressure occurs at frequencies near resonance, where the water motion and vessel roll reinforce each other, increasing the lateral force on the tank walls and potentially reducing the righting moment. Therefore, vessel operation near resonant frequencies should be avoided to prevent reduced stability. In this study the critical frequency is 2 rad/s.

3) Effect of Roll Angle

The following section explains the effect of θ variation on pressure distribution on the tank walls. The vessel's θ determines the extent to which the water mass shifts to one side of the tank, thereby influencing the dynamic load on the tank walls. Simulation analysis indicates that θ increase results in a higher inertial component of the water (lateral acceleration). Subsequently, dynamic pressure on the tank walls rises. The corresponding pressure trends are shown in Figure 11.

However, the pressure pattern is not always linear. At an H of 50% the wide free surface allows intensive sloshing, leading to complex pressure fluctuations on the tank walls. For instance, when θ increases from 5 ° to 10–15 °, the pressure at the upper wall points (L16–L21) temporarily drops drastically and then rises again at 20 °. This phenomenon is associated with phase lag between the vessel motion and the fluid, which shifts the positions of nodes and antinodes inside the tank [11]. This shift causes points that originally experienced the maximum pressure to become regions of the minimum pressure, resulting in a non-linear relationship between θ and dynamic pressure. This explains the non-monotonic behavior of dynamic pressure patterns at medium θ (10–15 °). In contrast, at an H of 90%, sloshing motion is more constrained. This behavior is attributed to the smaller free surface, resulting in a more regular pressure distribution dominated by hydrostatic pressure, with relatively small dynamic fluctuations, as displayed in Figures 11b and 12.

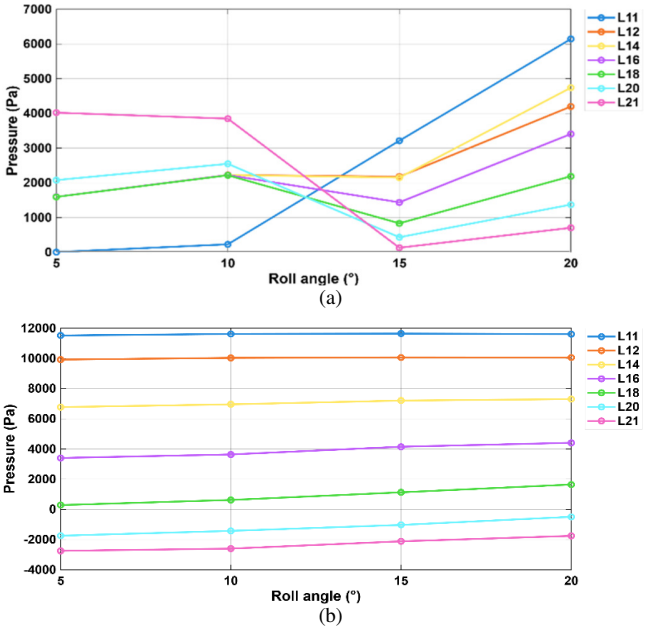

Fig. 11. θ against pressure for: (a) H of 50% and (b) H of 90% (roll frequency 1.519 rad/s).

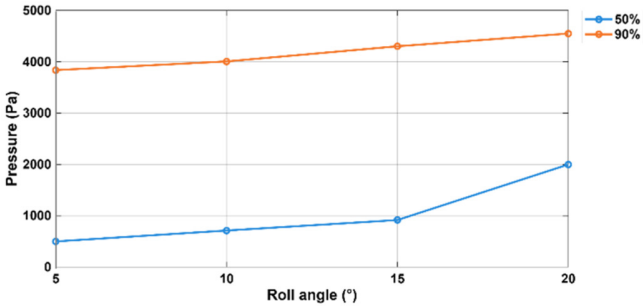

Fig. 12. θ and mean total pressure (roll frequency = 1.519 rad/s).

B. Heeling Moment

Figure 13(a) presents the M_h caused by water pressure on the tank walls for variations in tank H (Figure 13(a)) and the comparison between H and free surface width (Figure 13(b)). The results indicate that the M_h induced by dynamic water pressure on the tank walls due to vessel motion is directly proportional to the H in the tank as well as the ratio between the H and the tank's free surface width. This is consistent with the sloshing and stability theory [11]. Specifically, a higher H increases the M_h because the larger water mass generates more significant dynamic pressure on the tank walls opposite the vessel's restoring force. In the transitional filling range (50% and 70% of tank height), the pressure gradient increases gradually compared to low filling levels (10–50% of tank height) and high filling levels (70–90% of tank height). The gradient of M_h changes due to wall pressure. Figure 13(b) shows that the ratio of H to free surface width also affects the M_h, although less significantly than the H itself. These results indicate that variations in H and tank cross-sectional shape are important factors influencing sloshing-induced M_h in live-bait tanks.

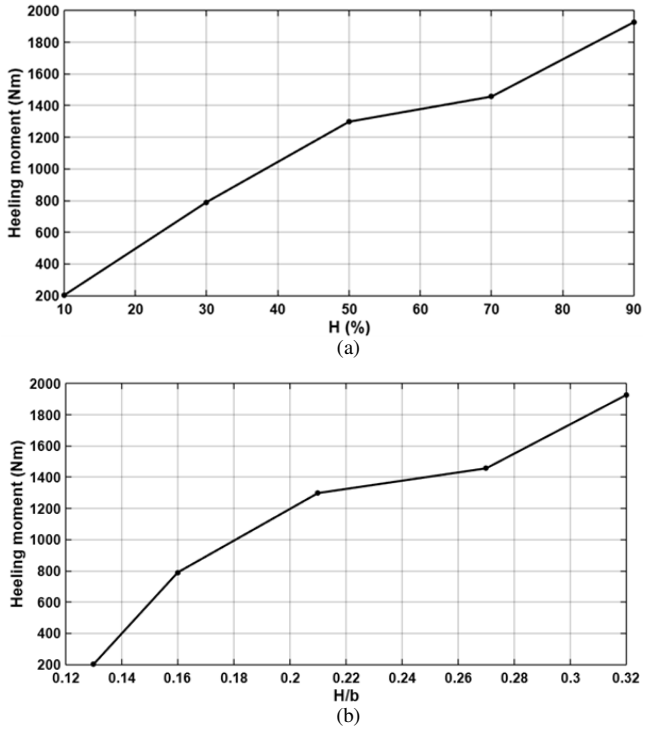

Fig. 13. M_h against: (a) H and (b) H/b (roll frequency = 1.519 rad/s and θ = 20 °).

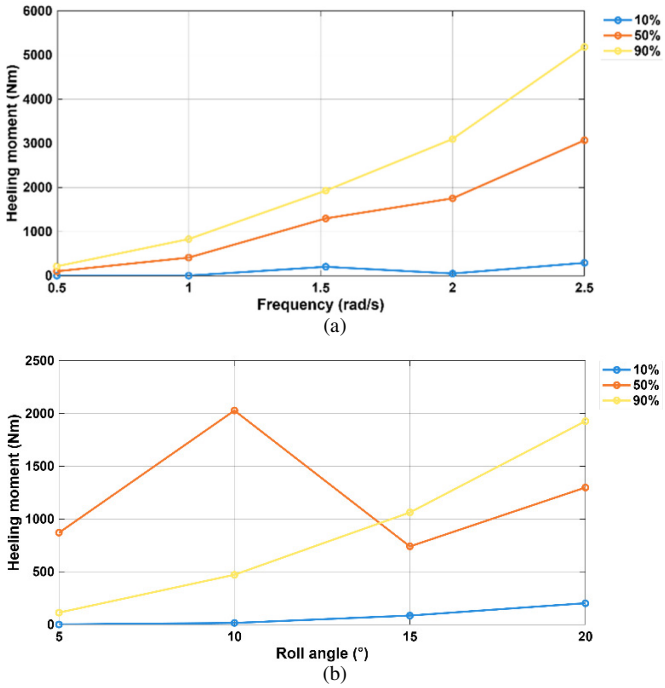

Fig. 14. M_h against: (a) rolling frequency and (b) θ.

The vessel's roll excitation frequency plays an important role in determining the magnitude of M_h resulting from the interaction between vessel motion and water dynamics inside the tank. Figure 14(a) presents the variation of M_h with vessel rolling frequency at three representative H: 10%, 50%, and 90%. Higher rolling frequencies induce larger M_h. A similar trend is observed for all filling levels. However, the influence of H becomes more significant at higher rolling frequencies. As rolling frequency increases, the velocity of vessel motion also rises, resulting in stronger water movement inside the tank. With a larger moving water mass at higher filling levels, the resulting dynamic pressure becomes greater. Therefore, the change in M_h due to H is more pronounced at higher rolling frequencies. Resonance effects [12, 31] are not significant in this case because the oscillating water volume is relatively small due to the tank's limited size. This is evident at 50% H and a rolling frequency of 1.519 rad/s, where the pressure gradient rises and then levels off at 2 rad/s. On the other hand, the M_h induced by sloshing depends heavily on the pressure distribution across the entire tank wall. Consequently, the tank resonance is not apparent, in contrast to the dynamic pressure variations with rolling frequency, as illustrated in Figures 9 and 10.

The vessel's θ significantly affects the M_h because it influences the displacement of water mass inside the tank. As the θ increases, the center of water mass moves farther from the vessel's center of gravity, increasing the moment arm and adding to the dynamic heeling load. In Figure 14(b), at an H of 10%, the M_h rises gradually and monotonically due to the small water volume limiting sloshing energy. At 90% H, the M_h increase is also stable and monotonic because sloshing is damped and dynamic pressure is dominated by the large inertial force of water. At a large θ (20 °), the M_h reaches its maximum, indicating that near-full tank conditions produce more controlled water response but result in a higher cumulative structural load on the vessel [19]. However, at 50% H, dynamic pressure is dependent on the sloshing wave pattern, as illustrated in Figure 14(b). Small changes in θ can shift the pressure peak to a different location (moving antinode), so a 10 ° roll can produce a dynamic pressure spike and peak M_h. The sharp variation of M_h at 10 ° is mainly caused by the increase in the resultant dynamic force, as shown in Figure 11(a). This behavior has been analyzed in [11], explaining the phase shift in sloshing and movement of pressure antinodes, where pressure peaks shift to different locations as the θ changes.

C. Stability Margin

Based on the M_h obtained in the previous analysis, the GZ_h due to tank water dynamics was statically calculated to evaluate the vessel's stability margin. Table II presents the GZ_h resulting from tank water dynamics induced by rolling motion at various H with different rolling frequencies and θ.

Across all simulated conditions, the GZ_h remains smaller than the GZ_r for all θ values. Nevertheless, this phenomenon should be considered, since pressure on the tank walls may act as an additional excitation moment, potentially increasing θ depending on the phase difference between the vessel's rolling motion and the water sloshing in the tank. Authors in [32] confirmed that within certain rolling frequency ranges, tank water dynamics can amplify θ. Regarding other frequency ranges, tank water dynamics act as a damper for rolling motion. Consequently, fully coupled simulations of ship motion and

tank sloshing are essential to investigate the interplay between tank geometry characteristics and vessel response under various operational conditions.

TABLE II. COMPARISON OF GZ_h AND GZ_r PER H, ROLLING FREQUENCY, AND θ

Variation	Parameter	GZ_h (m)	GZ_r (m)
H (%) (θ= 20 °)	10	0.0005	0.715
	30	0.002	0.715
	50	0.003	0.715
	70	0.004	0.715
	90	0.005	0.715
Frequency (rad/s) (θ= 20 °)	0.5 (H=50%)	0.0003	0.715
	0.5 (H=90%)	0.0005	0.715
	1.0 (H=50%)	0.001	0.715
	1.0 (H=90%)	0.002	0.715
	1.519 (H=50%)	0.003	0.715
	1.519 (H=90%)	0.005	0.715
	2.0 (H=50%)	0.004	0.715
	2.0 (H=90%)	0.008	0.715
	2.5 (H=50%)	0.008	0.715
	2.5 (H=90%)	0.013	0.715
θ (°)	5 (H=50%)	0.002	0.2125
	5 (H=90%)	0.0003	0.2125
	10 (H=50%)	0.005	0.425
	10 (H=90%)	0.001	0.425
	15 (H=50%)	0.002	0.57
	15 (H=90%)	0.003	0.57
	20 (H=50%)	0.003	0.715
	20 (H=90%)	0.005	0.715

The influence of tank condition variations and simulation scenarios on the GZ_h is consistent with the effect of tank dynamics on the M_h, since the GZ_h is defined as the M_h divided by the vessel's displacement. The maximum GZ_h occurs for an H of 90%, a θ of 20 °, and a roll frequency of 2.5 rad/s. For higher roll frequencies, the analysis shows that for each H condition, including shallow (10–30%), medium (50–70%), and nearly full (90%), the difference between GZ_h and GZ_r remains significant. For instance, at an H of 90% and a θ of 20 °, GZ_h reaches only ~0.0048 m, while GZ_r reaches 0.715 m. This indicates that the effects of free surface and sloshing on vessel stability are limited to reducing the stability margin slightly and do not compromise the vessel's righting capability.

Comparison across roll excitation frequencies in Table II highlights that increasing frequency tends to increase GZ_h. For instance, at an H value of 50%, GZ_h increases when approaching the resonance frequency. However, in all cases, GZ_r derived from the stability curve remains higher. This result confirms that although high frequencies increase the dynamic response of water and contribute to an increased GZ_h, the vessel retains sufficient righting capability. Therefore, resonance effects increase oscillation load without reducing stability.

Regarding variations in θ, GZ_h increases with larger angles due to greater water motion, but it still does not exceed GZ_r. For example, at θ equal to 10 °, GZ_h is only a few mm (5 mm at H = 50% and 1 mm at H = 90%), whereas GZ_r remains 42.5 cm. Therefore, large θ provide water with more freedom to move and exert pressure on the tank walls; thus, the vessel's righting moment still dominates overall stability maintenance. Overall, the comparison of GZ_h and GZ_r demonstrates that the M_h generated by sloshing reduces the stability margin without exceeding the ship's righting capability. Consequently, the vessel continues to satisfy intact stability requirements and maintains an adequate safety margin against the dynamic effects of tank water [33].

IV. CONCLUSIONS

The present study demonstrates that variations in the H within the live-bait tank significantly affect both the distribution of hydrostatic and dynamic pressures and the vessel's heeling moments (M_h). The highest dynamic pressure occurs near the free surface of the tank, where water velocity is maximal. The effects of roll excitation frequency and roll angle (θ) on the tank wall pressure are the most pronounced at medium to low water filling levels (H). At a near-full filling level (H = 90%), variations in pressure due to changes in frequency and θ are relatively minor compared to the fluctuations observed at lower H.

The M_h induced by fluid motion inside the live-bait tank increases with higher H and with the ratio of free surface height to tank width. The gradient of M_h change tends to decrease during the transition of H from 50% to 70% and from a free surface height-to-width ratio of 0.21 to 0.27. The M_h further increases with higher roll excitation frequencies. However, for $H \leq 50\%$, a change in the growth gradient is observed at a rolling frequency of 1.519 rad/s. θ values of 10 ° or smaller and H equal to 50% significantly affect the disturbing moment. The maximum GZ_h of 0.013 m occurs for an H of 90% with a roll amplitude of 20 ° and a roll frequency of 2.5 rad/s. With a GZ_r of 0.715 m at a θ of 20 °, the vessel maintains sufficient stability to counteract the M_h generated by water motion within the tank up to 20 °.

This study fills a gap in the existing sloshing research for fishing vessels with hull-shaped tanks, where studies remain limited. It also provides new insights into the relationship between roll frequency and H on the M_h, particularly at conditions approaching resonance (1.519–2 rad/s) and at medium filling levels (50–70%). The results of this study can assist naval architects to determine the optimal water level in the live-bait tank and identify conditions to avoid maintaining sufficient dynamic stability.

A limitation of this study is that the simulations were confined to the tank domain, and the fully coupled interaction between vessel motion and tank sloshing was not analyzed. Future research could focus on tank geometries with baffles, variations in live fish cargo, experimental validation, and extending the range of parameters, including tank geometry and realistic sea conditions.

ACKNOWLEDGMENT

This paper is a part of the research conducted with the support of the Directorate of Research, Technology and Community Service of the Ministry of Higher Education, Science and Technology of Indonesia under the skim of Fundamental Research (02209/UN4.22/PT.01.03/2025).

REFERENCES

[1] E. Esteves and J. Aníbal, "Muxama and other traditional food products obtained from tuna in south Portugal and Spain: review and future perspectives," *Journal of Ethnic Foods*, vol. 6, Dec. 2019, Art. no. 18, https://doi.org/10.1186/s42779-019-0022-6.

[2] P. M. Silva, C. Pita, and C. M. Teixeira, "Two Realities in the Portuguese Tuna Fishery: What Happens in the Largest EEZ of European Union?," *Regional Studies in Marine Science*, vol. 77, Dec. 2024, Art. no. 103719, https://doi.org/10.1016/j.rsma.2024.103719.

[3] R. Gillett, "Pole-and-Line Tuna Fishing in the World: Status and Trends," International Pole & Line Foundation, London, United Kingdom, Technical Report 6, 2015.

[4] C. Litaay, D. D. Pelasula, S. M. Horhoruw, and H. Arfah, "Effect of Bait Availability on Pole and Line Fisheries and the Impact on the Amount of Fish Consumption," in *IOP Conference Series: Earth and Environmental Science*, Aug. 2020, vol. 763, Art. no. 012048, https://doi.org/10.1016/j.rsma.2024.103719.

[5] Y. Novita, A. D. Ramadhan, and M. Imron, "Influence of Free Surface Area of Liquid Cargo Towards Rolling Motion of a Ship Model," *Journal of Fisheries Science and Technology*, vol. 8, no. 2, pp. 44–51, Nov. 2012.

[6] P. R. Couser, "On The Effect of Tank Free Surfaces On Vessel Static Stability," *The International Journal of Maritime Engineering*, vol. 146, Art. no. a3, 2004, https://doi.org/10.3940/rina.ijme.2004.a3.24041.

[7] P. Krata, "The Impact of Sloshing Liquids on Ship Stability for Various Dimensions of Partly Filled Tanks," *TransNav - The International Journal on Marine Navigation and Safety of Sea Transportation*, vol. 7, pp. 481–489, 2013, https://doi.org/10.12716/1001.07.04.02.

[8] L. Liu, D. Feng, X. Wang, Z. Zhang, J. Yu, and M. Chen, "Numerical study on the effect of sloshing on ship parametric roll," *Ocean Engineering*, vol. 247, Mar. 2022, Art. no. 110612, https://doi.org/10.1016/j.oceaneng.2022.110612.

[9] Z. Zhang, Q. Wu, Y. Xie, and H. Yu, "Experimental and numerical investigations on the liquid tank sloshing in regular waves," *Ocean Engineering*, vol. 271, Mar. 2023, Art. no. 113668, https://doi.org/10.1016/j.oceaneng.2023.113668.

[10] X. Sun, Y. Zhong, F. Bian, C. Liu, and Y. Yin, "Numerical Computation of Sloshing-Induced Force in Complex Ship Tanks under the Excitation of Ship Rolling Motion Based on the MPS Method," *Applied Sciences*, vol. 12, no. 10, Jan. 2022, Art. no. 5130, https://doi.org/10.3390/app12105130.

[11] X. Fan, Z. Hu, and X. Zheng, "Research on Influence of Tank Sloshing on Ship Motion Response under Different Wavelengths," *Applied Sciences*, vol. 12, no. 17, Aug. 2022, Art. no. 8647, https://doi.org/10.3390/app12178647.

[12] J. Jiao, S. Ding, M. Zhao, M. Jiang, S. Bu, and Y. Shi, "Simulation of LNG ship's motions coupled with tank sloshing in regular waves by DualSPHysics," *Ocean Engineering*, vol. 312, Nov. 2024, Art. no. 119148, https://doi.org/10.1016/j.oceaneng.2024.119148.

[13] W. Lyu, O. el Moctar, and T. E. Schellin, "Ship motion-sloshing interaction with forward speed in oblique waves," *Ocean Engineering*, vol. 250, Apr. 2022, Art. no. 110999, https://doi.org/10.1016/j.oceaneng.2022.110999.

[14] D. A. Prassyeta, E. S. Hadi, and G. Rindo, "Pengaruh Variasi Bentuk Perforated Pada Floating Baffles Untuk Mengurangi Efek Sloshing Pada Palka Kapal Ikan Tradisional 30 Gt Di Daerah Batang – Jawa Tengah," *Jurnal Teknik Perkapalan*, vol. 4, no. 2, Apr. 2016.

[15] M. A. Azis, "Stability Assessment of Traditional Wooden Ships According to the International Stability Criteria," Master's Dissertation, Hasanuddin University, Dept. of Naval Architecture, Makassar, Indonesia, 2020.

[16] A. R. Prakarsa, D. Chrismianto, and M. Iqbal, "Analisa Pengaruh Sloshing Pada Ruang Muat Kapal Tanker Pertamina 17500 LTDW Dengan Metode CFD (Computational Fluid Dynamic)," *Jurnal Teknik Perkapalan*, vol. 5, no. 1, Jan. 2011.

[17] A. Ma'ruf, D. Paroka, and H. Palippui, "Analysis Of The Influence Of Total Content On Tank Sloshing Load On Tanker Vessels Using Numeric Method," *Zona Laut Jurnal Inovasi Sains Dan Teknologi Kelautan*, pp. 7–13, Mar. 2021, https://doi.org/10.62012/zl.v2i1.13340.

[18] G. K. Batchelor, *An Introduction to Fluid Dynamics*. New York, NY, USA: Cambridge University Press, 2000.

[19] F. R. Menter, R. B. Langtry, S. R. Likki, Y. B. Suzen, P. G. Huang, and S. Völker, "A Correlation-Based Transition Model Using Local Variables—Part I: Model Formulation," *Journal of Turbomachinery*, pp. 413–422, Mar. 2004, https://doi.org/10.1115/1.2184352.

[20] M. Iqbal, M. Terziev, T. Tezdogan, and A. Incecik, "Unsteady RANS CFD Simulation on the Parametric Roll of Small Fishing Boat under Different Loading Conditions," *Journal of Marine Science and Application*, vol. 23, no. 2, pp. 327–351, May 2024, https://doi.org/10.1007/s11804-024-00427-0.

[21] D. E. Setiawan, B. H. Iskandar, F. Purwangka, V. R. Kurniawati, and A. Purbayanto, "Placement Planning of a Powered Cooling Engine on a 5 < Gross Tonnage Fishing Vessel," *Engineering, Technology & Applied Science Research*, vol. 15, no. 3, pp. 23169–23176, June 2025, https://doi.org/10.48084/etasr.10609.

[22] L. Hou, F. Li, and C. Wu, "A numerical study of liquid sloshing in a two-dimensional tank under external excitations," *Journal of Marine Science and Application*, vol. 11, no. 3, pp. 305–310, Sept. 2012, https://doi.org/10.1007/s11804-012-1137-y.

[23] I. Ghamari, H. R. Mahmoudi, A. Hajivand, and M. S. Seif, "Ship Roll Analysis Using CFD-Derived Roll Damping: Numerical and Experimental Study," *Journal of Marine Science and Application*, vol. 21, pp. 67–79, Apr. 2022, https://doi.org/10.1007/s11804-022-00254-1.

[24] X. Vallés Rebollo, E. Sadeghi, I. Kusano, and A.-A. García-Granada, "Study of the Sloshing Dynamics in Partially Filled Rectangular Tanks with Submerged Baffles Using VOF and LES Turbulence Methods for Different Impact Angles," *Computation*, vol. 10, no. 12, Dec. 2022, Art. no. 225, https://doi.org/10.3390/computation10120225.

[25] B. Bäuerlein and K. Avila, "Phase lag predicts nonlinear response maxima in liquid-sloshing experiments," *Journal of Fluid Mechanics*, vol. 925, Oct. 2021, Art. no. A22, https://doi.org/10.1017/jfm.2021.576.

[26] Q. Zhang, B. Shui, and H. Zhu, "Study on Sloshing Characteristics in a Liquid Cargo Tank under Combination Excitation," *Journal of Marine Science and Engineering*, vol. 10, no. 8, Aug. 2022, Art. no. 1100, https://doi.org/10.3390/jmse10081100.

[27] Y. K. Song, K.-A. Chang, Y. Ryu, and S. H. Kwon, "Experimental study on flow kinematics and impact pressure in liquid sloshing," *Experiments in Fluids*, vol. 54, no. 9, Sept. 2013, Art. no. 1592, https://doi.org/10.1007/s00348-013-1592-5.

[28] K. Liu, X. Li, P. Peng, Z. Zhou, and Z. Gao, "Experimental Study on the Sloshing of a Rectangular Tank under Pitch Excitations," *Water*, vol. 16, no. 11, May 2024, Art. no. 1551, https://doi.org/10.3390/w16111551.

[29] S. K. Kleivane and B. J. Leira, "Effect of sloshing on a local structural system in a partially filled tank," *Applied Ocean Research*, vol. 164, Nov. 2025, Art. no. 104763, https://doi.org/10.1016/j.apor.2025.104763.

[30] A. Kamath, E. L. Grotle, and H. Bihs, "Numerical Investigation of Sloshing Under Roll Excitation at Shallow Liquid Depths and the Effect of Baffles," *Journal of Marine Science and Application*, vol. 20, no. 2, pp. 185–200, June 2021, https://doi.org/10.1007/s11804-021-00198-y.

[31] Y. Qiu, M. Bai, Y. Liu, G. Lei, and Z. Liu, "Effect of liquid filling level on sloshing hydrodynamic characteristic under the first natural frequency," *Journal of Energy Storage*, vol. 55, Nov. 2022, Art. no. 105452, https://doi.org/10.1016/j.est.2022.105452.

[32] X. Yuan, Y. Su, and P. Xie, "Frequency Characteristics of Sloshing Resonance in a Three-Dimensional Shallow-Water Rectangular Tank," *Journal of Marine Science and Engineering*, vol. 10, no. 11, Nov. 2022, Art. no. 1792, https://doi.org/10.3390/jmse10111792.

[33] International Maritime Organization, "Resolution MSC.267(85): Adoption of the International Code on Intact Stability, 2008 (2008 IS Code)," International Maritime Organization, London, United Kingdom, Resolution MSC.267(85), 2008.